Journal of Power Sources 245 (2014) 183–193

Contents lists available at SciVerse ScienceDirect

Journal of Power Sources

journal homepage: www.elsevier.com/locate/jpowsour

Role of V_2O_5 coating on $LiNiO_2$-based materials for lithium ion battery

Xunhui Xiong, Zhixing Wang*, Guochun Yan, Huajun Guo, Xinhai Li

School of Metallurgical Science and Engineering, Central South University, Changsha 410083, PR China

HIGHLIGHTS

- V_2O_5 is investigated as coating material on $LiNiO_2$-based material.
- Coating layer works as HF inhibitor and HF scavenger when contacted with electrolyte.
- V_2O_5 delays Ni^{3+}/Ni^{2+} transformation and lithium extraction.
- The improvements in storage in air benefit from the unique properties of V_2O_5.

GRAPHICAL ABSTRACT

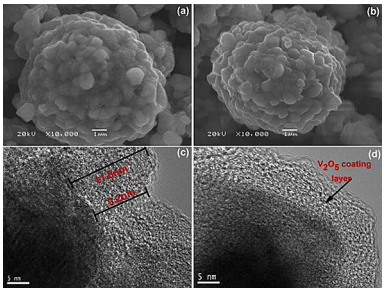

ARTICLE INFO

Article history:
Received 26 April 2013
Received in revised form
13 June 2013
Accepted 24 June 2013
Available online 1 July 2013

Keywords:
Lithium ion battery
Lithium nickel oxide-based materials
Vanadium pentoxide coating
Electrochemical performance
Storage characteristic

ABSTRACT

X-ray diffraction (XRD), transmission electron microscope (TEM), energy dispersive spectrometer (EDX) and X-ray photoelectron spectroscopy (XPS) are used to demonstrate that V_2O_5 is successfully coated on $LiNiO_2$-based materials. The V_2O_5 layer will react with Li impurities on surface, which will reduce the pH value and rapid moisture uptake ability of $LiNiO_2$-based materials. Cells tests indicate that V_2O_5-coating layer works as HF inhibitor and/or HF scavenger, which contributes a significant improvement in cycling performance and storage characteristics in electrolyte. In the mean time, V_2O_5 acts as isolating layer when cathode material contacts with electrolyte especially cycling at high voltage. Structural analysis shows that V_2O_5-coating layer has more advantage over other oxide coating in delaying Ni^{3+}/Ni^{2+} transformation and lithium extraction from bulk surface, which benefits from the properties of V_2O_5 reacting with $LiOH/Li_2CO_3$ impurities on surface.

1. Introduction

There has been a significant interest in the synthesis, structure, and electrochemical properties of lithiated transition metal oxides due to their use as positive electrodes in lithium-ion batteries. Layered $LiNi_xM_{1-x}O_2$ (M = metal) materials have been intensively studied as potential cathode materials for application in electric vehicles (EV) and plug-in hybrid electric vehicles (P-HEVs) [1–4]. It is reported $LiNi_xM_{1-x}O_2$ materials inherit the merits of mono metal oxide $LiCoO_2$, $LiNiO_2$ and $LiMnO_2$, and the layered Ni-rich layered cathode materials have been considered as promising candidate due to their large capacity, excellent rate capability and low cost [5–7]. However, the rapid moisture uptaking ability of Ni-rich ($x \geq 0.8$) materials stemmed from the slow and spontaneous reduction of Ni^{3+} to Ni^{2+} and physical/chemical adsorption of synthetic residue $Li_2O/LiOH$ on surface has been the problem to overcome [8–11]. G.V. Zhuang et al. observed a 10 nm Li_2CO_3 layer after exposed to air for 2 years, and part of Li_2CO_3 was formed by the reaction of atmospheric H_2O/CO_2 with lithium oxide residue on surface [8]. K. Shizuka et al. found that the first step in the carbonation reactions occurs with the excess Li components on surface, Li_2O for example [11]. Except for physical adsorption of residue $Li_2O/LiOH$, a reduction of Ni^{3+} to Ni^{2+} also happened on the particle surface which resulted in forming LiOH, $LiHCO_3$, Li_2CO_3 and

* Corresponding author. Tel./fax: +86 731 88836633.
E-mail address: xxhui881118@126.com (Z. Wang).

0378-7753/$ – see front matter © 2013 Elsevier B.V. All rights reserved.
http://dx.doi.org/10.1016/j.jpowsour.2013.06.133

NiO-like layer when $LiNiO_2$-based materials are exposed to air [12,13]. Both Li_2CO_3 and LiOH impurities formed on the cathode's surface will worsen its machining performance and electrochemical performance.

One practicable way to solve the rapid moisture uptaking problem of $LiNiO_2$-based cathode materials may coat their surfaces with nano-scale layers of lithium-reactive material such as $Co_3(PO_4)_2$ [14,15]. $Co_3(PO_4)_2$ will react with lithium impurities ($LiOH/Li_2CO_3$) and trace Li in the bulk layer after annealing at 700 °C, which lowers the pH value of $LiNiO_2$-based materials and avoids physical adsorption of residue $Li_2O/LiOH$. Besides, Li_xCoPO_4 and unreacted $Co_3(PO_4)_2$ can also act as a physical protection layer to prevent or suppress the reduction reaction between cathode materials and air. Moreover, $Li_xCoPO_4/Co_3(PO_4)_2$ are thermally stable even after full delithation, thus minimizing any side reactions with electrolytes.

On the other hand, in attempts to increase the reversible capacity of the $LiNiO_2$-based material, the upper cutoff voltage limit has been progressively raised. However, the electrode charged to a high voltage (≥4.5 V) leads to a significant deterioration of the cycle performance. The origin of this capacity fading is related to the increase in the surface reactivity between the highly delithiated and instable cathode and the electrolyte, resulting in significant interfacial impedance rise. Extensively studies have been made about metal oxides coating (such as Al_2O_3, ZrO_2 and TiO_2) for lithiated transition metal oxide to improve cycle performance and rate capability under a high cutoff voltage [16–18]. Until now, there are no reports about the effect of surface modification of $LiNiO_2$-based materials by V_2O_5 on electrochemical performance at a high cutoff voltage.

Recent research progresses prove that amorphous vanadium oxides have become one of the most attractive candidates as coating material for it acts as an ion and electrons double conductive materials [19–22]. Park et al. reported that VO_x impregnated $0.5Li_2MnO_3 \cdot 0.5LiNi_{0.4}Co_{0.2}Mn_{0.4}O_2$ cathode materials showed an improved electrochemical performance for the vanadium ions in $3d^0$ electronic states during high voltage charging state could reduce the surface catalytic activities and stabilize the surface oxide ions during their electrochemical oxidation [19]. Lee et al. reported that a vanadium oxide coating layer on $LiCoO_2$ improved the cycleability at a high-charge cut-off voltage [20]. J. Cho et al. reported V_2O_5-coated TiO_2 demonstrated a superior rate capability due to the better electrical conductivity and fast Li-ion diffusion [21]. In our previous report, V_2O_5 coating is also introduced to enhance the cycling performance and structural stability $LiNiO_2$-based materials. The coating layer can suppress the dissolution of transition metal from layer $LiNi_{0.8}Co_{0.1}Mn_{0.1}O_2$ [23]. In the present study, we have explored the possibility of V_2O_5 coating in improving the storage properties in air and performance of cut off voltage. With the help of the acidic isolated layer and the removal of lithium impurities on surface by V_2O_5, poor performance at high voltage and storage characteristics are expected to be resolved. Here, taking $LiNi_{0.8}Co_{0.1}Mn_{0.1}O_2$ as an example, the role of coating layer suppressing the propagation of HF, the improving the storage properties in air and enhancement of cut off voltage is discussed in detail.

2. Experimental

$LiNi_{0.8}Co_{0.1}Mn_{0.1}O_2$ powder was prepared by mixing co-precipitated $Ni_{0.8}Co_{0.1}Mn_{0.1}(OH)_2$ and $LiOH \cdot H_2O$ at a molar ratio of 1:1.05, and firing at 480 and 750 °C in O_2 flow for 5 and 15 h, respectively. To prepare V_2O_5-coated $LiNi_{0.8}Co_{0.1}Mn_{0.1}O_2$, 1.457 g vanadiumoxy acetylacetonate ($C_{10}H_{14}O_5V$) was dissolved in 100 mL ethanol at 90 °C accompanied by adding 100 g of $LiNi_{0.8}Co_{0.1}Mn_{0.1}O_2$. The suspension was dried and annealed at 400 °C for 3 h in air.

To prepare the cathode, the active material, poly(vinylidene fluoride) and carbon black were blended at a ratio of 8:1:1. The mixture was dispersed in *N*-pyrrolidinone (NMP) and the resultant slurry was coated onto Al foil using the Doctor-Blade technique. After drying at 120 °C under vacuum for 12 h, the electrodes were assembled into CR2025 coin-type cells with a Li electrode and electrolyte (1 M $LiPF_6$ in EC: EMC: DMC = 1: 1: 1 in volume) in an Ar-filled glove box. The cells were cycled galvanostatically between 2.8 and 4.3–4.5 V (vs. Li/Li^+) at a desired current density.

For HF titration, the cycled cells were carefully disassembled and all contents of the cell washed thoroughly with DMC for one week in the glove box. 0.01 mol L^{-1} NaOH aqueous solution and Bromothymol Blue (BTB, Aldrich) as an indicating solution were used for the titration of the extensively cycled electrolyte.

The crystal structure of the products was confirmed by X-ray powder diffraction (XRD, Rint-2000, Rigaku) using Cu-Kα radiation (1.54056 Å). The morphology of the particles was measured by scanning electron microscope (JEOL, JSM-5612LV) with an accelerating voltage of 20 kV, and by transmission electron microscope (Tecnai G12, 200 kV). X-ray photoelectron spectroscopy (XPS, PHI 5600, Perkin–Elmer) measurements were performed to get information on the surface of V_2O_5-coated $LiNi_{0.8}Mn_{0.1}Co_{0.1}O_2$.

3. Results and discussion

Prior to investigating cell performance and storage characteristics of $LiNi_{0.8}Mn_{0.1}Co_{0.1}O_2$, we first conducted structural characterization of V_2O_5-coated $LiNi_{0.8}Mn_{0.1}Co_{0.1}O_2$. Fig. 1(a) and (b) exhibits the XRD pattern and Rietveld refinement results of the pristine and V_2O_5-coated sample. The results reveal that both samples have typical layered structure of α-$NaFeO_2$ type with space group $R\bar{3}m$. This suggests that the crystal structure of $LiNi_{0.8}Co_{0.1}Mn_{0.1}O_2$ is not affected by the V_2O_5 coating. The absence of diffraction patterns corresponding to V_2O_5 compounds may be due to the fact that V_2O_5 is amorphous phase and/or the low concentration of V_2O_5 compared with $LiNi_{0.8}Co_{0.1}Mn_{0.1}O_2$. This is further confirmed by Rietveld analysis. The lattice constants for pristine (a = 2.8711 Å, c = 14.1969 Å) and coated material (a = 2.8709 Å, c = 14.1966 Å) estimated by Rietveld analysis imply the V_2O_5 is amorphous and is not incorporated into the host structure due to the low calcination temperature.

Fig. 2(b) shows that, in comparison with pristine sample having smooth surface and well-defined edges (an inset is a TEM image), the coated sample is successfully coated with an apparently continuous layer. This coating layer was further examined by carried out HRTEM characterization. Fig. 2(c) shows that $LiNi_{0.8}Mn_{0.1}Co_{0.1}O_2$ is well covered by a layer approximately 6–10 nm. The inner layer of coating material is not easy to distinguish from the bulk phase because of the reaction between Li impurity on surface and V_2O_5 at 400 °C, and the outer layer could be a porous structure comparing to the active material.

In addition to these morphological results, the presence of the V_2O_5 layer on the $LiNi_{0.8}Mn_{0.1}Co_{0.1}O_2$ surface was also confirmed by observing an EDS image (Fig. 2(d)). The bright dots assigned to V elements of the V_2O_5 layer are uniformly dispersed on the $LiNi_{0.8}Mn_{0.1}Co_{0.1}O_2$ surface except very few isolated V_2O_5 particles. Schematic representations illustrating the V_2O_5 layer on the $LiNi_{0.8}Mn_{0.1}Co_{0.1}O_2$ surface and its function as an unusual protection skin to alleviate unwanted interfacial side reactions between $LiNi_{0.8}Mn_{0.1}Co_{0.1}O_2$ and liquid electrolytes or air are provided in Fig. 3.

XPS is an effective method that can provide an elemental analysis of the surface film with specific information on the

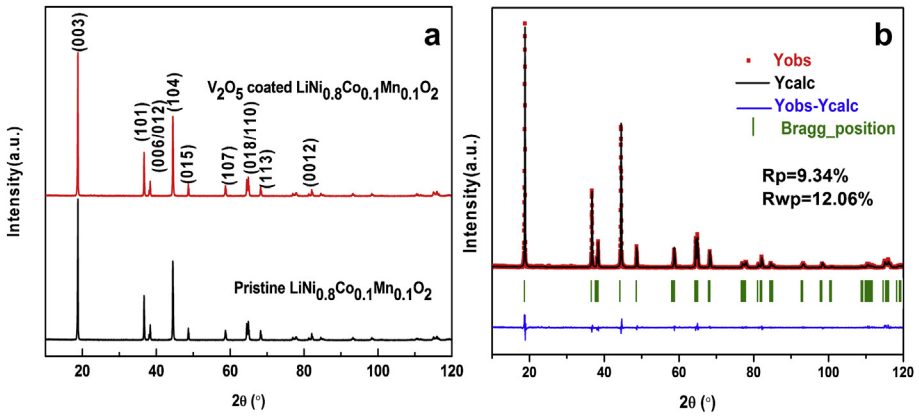

Fig. 1. The XRD patterns (a) and Rietveld refinements (b) of pristine and V_2O_5-coated sample.

oxidation states of the elements. Thus XPS analysis of the V_2O_5-coated $LiNi_{0.8}Co_{0.1}Mn_{0.1}O_2$ was carried out and the V2p XPS spectrum is given in Fig. 4. The observed binding energies of the V2p1/2 and V2p3/2 are 525.1 and 517.2 eV, respectively, which are very close to the values of V_2O_5 (524.95 and 517.45 eV). This result visually shows that the V element on the material surface is pentavalent. The C1s spectrum showed peaks at 284.7 and 289.3 eV. The 284.7 eV peak was attributed to "adventitious carbon" that is always present in the analysis chamber, while the 289.3 eV peak is attributed to a carbonate compound. The observation of Li_2CO_3 on the powder particle surface agrees with the results of previous investigations. The O1s peak of coated sample at low binding energy almost can be negligible. This verifies that the coating layer will consume the Li residual which is coincided with the change of pH value. Also, Li_2CO_3 specie is also clearly visible in the O1s spectra, where deconvolution reveals two oxygen environments. One is located at 529.5 eV, which can be assigned to the lattice oxygen in the metal framework [24–26]. Another peak is located at the higher binding energy of 531.1 eV. This peak can be assigned to the impurity of adsorbed species such as LiOH or Li_2CO_3 [27]. Compared with pristine sample, the O1s peak of coated sample at low binding energy is significantly reduced; in addition, the peak at 530.2 eV (corresponding to V_2O_5) is also dominant in the O1s spectrum. These all can demonstrate that V_2O_5 is successfully coated on the surface of $LiNi_{0.8}Co_{0.1}Mn_{0.1}O_2$ and V_2O_5 will consume the Li impurities during annealing. In the Ni2p spectra, the peaks of both samples are identical which can partly elucidate no changes happened in the bulk phase.

Fig. 5(a) exhibits the initial charge/discharge curves of pristine and V_2O_5-coated sample by applying a constant current of 20 mA g^{-1} (0.1 C rate) between 2.8 and 4.3 V. Clearly, V_2O_5-coated $LiNi_{0.8}Co_{0.1}Mn_{0.1}O_2$ delivers a similar discharge capacity with pristine sample at 201 mAh g^{-1}. The identical and smooth curves demonstrate V_2O_5 is not introduced into the bulk of the

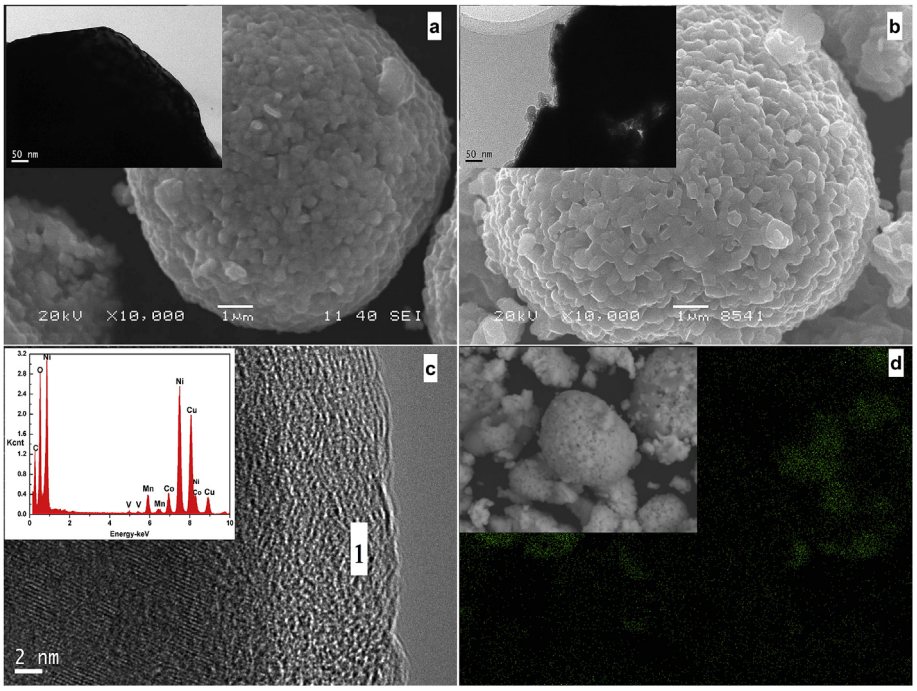

Fig. 2. Typical SEM and TEM images of pristine (a) and coated material (b); (c) HRTEM images of coated material and EDX of the selected area 1 in (c); (d) EDS mapping patterns of V on V_2O_5-coated $LiNi_{0.8}Co_{0.1}Mn_{0.1}O_2$.

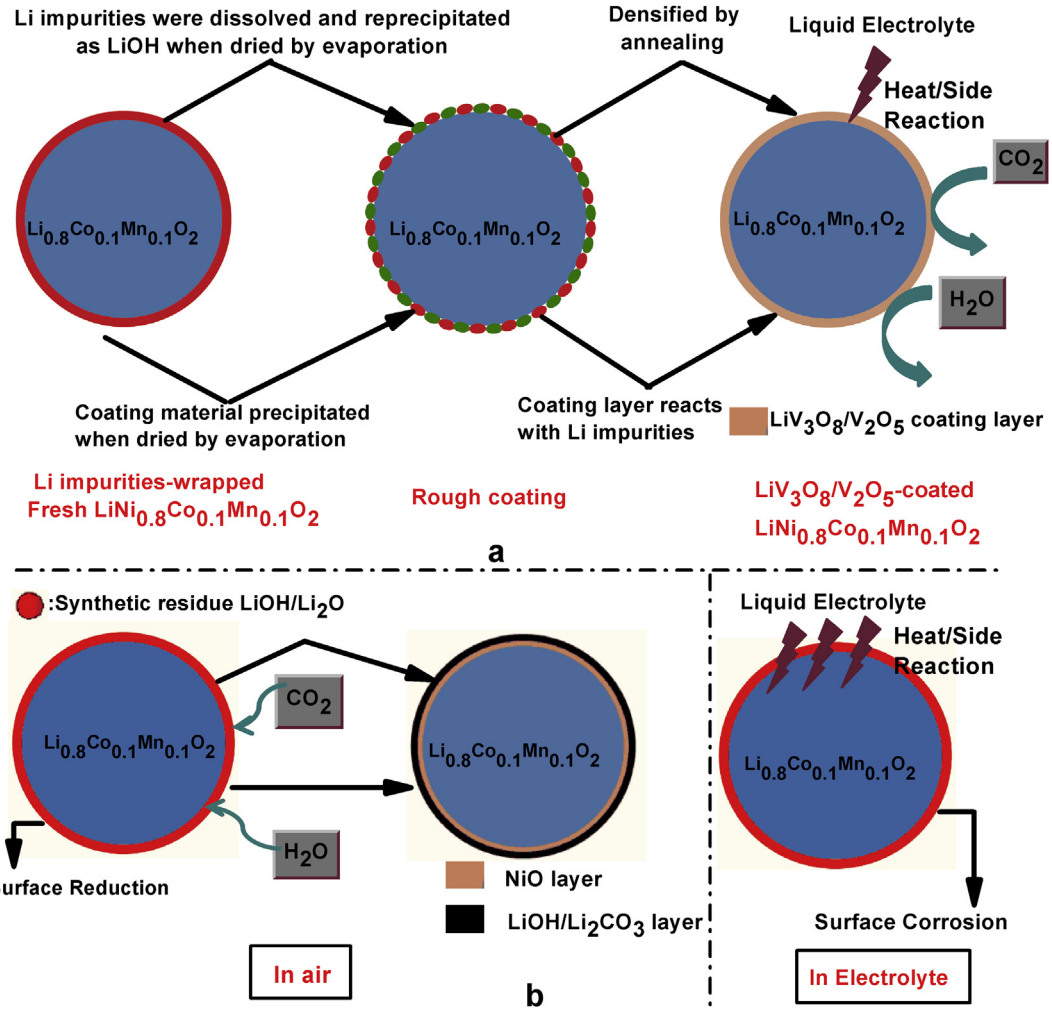

Fig. 3. Schematic illustrations of LiV_3O_8/V_2O_5 coating layer formed onto $LiNi_{0.8}Mn_{0.1}Co_{0.1}O_2$ and its function as a protection skin to suppress the unwanted interfacial side reactions.

$LiNi_{0.8}Co_{0.1}Mn_{0.1}O_2$ structure. In addition, the V_2O_5-coated sample almost delivers higher discharge capacities than the pristine sample at all the tested *C* rates, especially at high rates (Fig. 5(b)). Therefore, ionic and electronic transport through the nano-architectured coating layer consequently don't have a detrimental influence on the discharge capacities and C-rate capability of $LiNi_{0.8}Co_{0.1}Mn_{0.1}O_2$. The cycling performance of the two materials at a current rate of 400 mA g^{-1} is investigated and is shown in Fig. 5(c). The initial capacity of the V_2O_5-coated $LiNi_{0.8}Co_{0.1}Mn_{0.1}O_2$ is 171 mAh g^{-1}, as compared to that of pristine one having 170.6 mAh g^{-1}. However, the capacity retention of V_2O_5-coated sample is remarkably enhanced showing capacity loss of only 32.3% after 300 cycles, while the pristine electrode suffers from 50.7% capacity loss. The discharge curves of the first cycle and 300th cycle at 2C rate are shown in Fig. 5(d). The V_2O_5-coated sample displays a similar polarization at the first cycle, after 300 cycles, the pristine electrode shows a much higher polarization compared to the coated one. These poor cycling performances of the pristine $LiNi_{0.8}Co_{0.1}Mn_{0.1}O_2$ can be attributed to its vigorous surface reactivity with liquid electrolyte and the nanostructured coating layer work as isolating layer, which effectively protects the $LiNi_{0.8}Co_{0.1}Mn_{0.1}O_2$ surface from attack of the violent liquid electrolyte.

The cells extensively cycled are carefully disassembled, and all contents are soaked thoroughly in DMC solvent for one week in the glove box. The amount of HF in DMC analyzed by HF titration is about 253.5 ppm for the pristine material and 152.3 ppm for the V_2O_5-coated material. Fig. 6 demonstrates SEM images of separators selected from another cycled cells after 300 cycles. As seen in Fig. 6(a), white particle compounds cover most of the separator of the pristine material. However, a much small area is covered by the compounds for the case of the separator of V_2O_5-coated material in Fig. 6(c). EDX results (Fig. 6(b) and (d)) from such compounds indicate that the white particles may be the decomposition products of $LiPF_6$ such as LiF, POF_3 and Li_xPOF_y. The decomposition process of $LiPF_6$ follows the following reaction, as suggested by Aurbach et al. and Edström et al. [28,29]:

$$LiPF_6 \rightarrow LiF\downarrow + PF_5 \quad (1)$$

$$PF_5 + H_2O \rightarrow POF_3 + 2HF \quad (2)$$

$$POF_3 + Li_2O^- \rightarrow LiF\downarrow + Li_xPOF_y \quad (3)$$

As shown above, the Li impurity such as Li_2O will accelerate these reactions for pristine material. Furthermore, LiF and Li_xPOF_y type compounds which are highly resistive to Li^+ migration cause quite more increase in resistance after extensive cycles, leading to inferior cycleability. However, the V_2O_5 coating layer will react with Li impurity and less byproduct and HF will produce for V_2O_5-coated material. That is to say, V_2O_5 coating layer also works as an HF

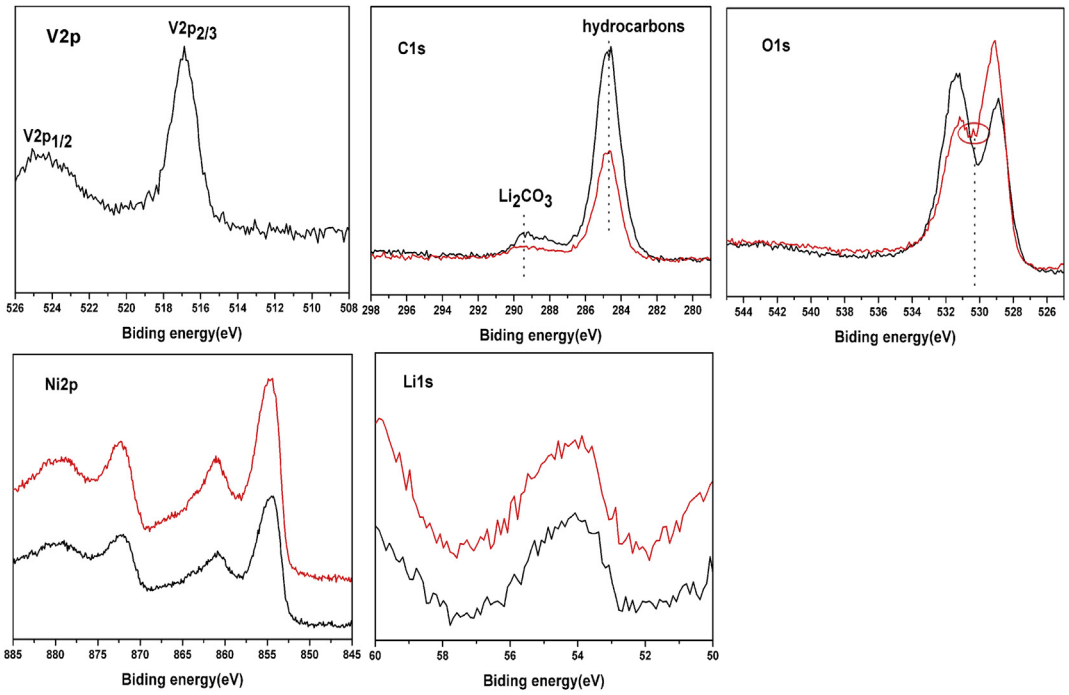

Fig. 4. XPS spectra of pristine and V_2O_5-coated sample.

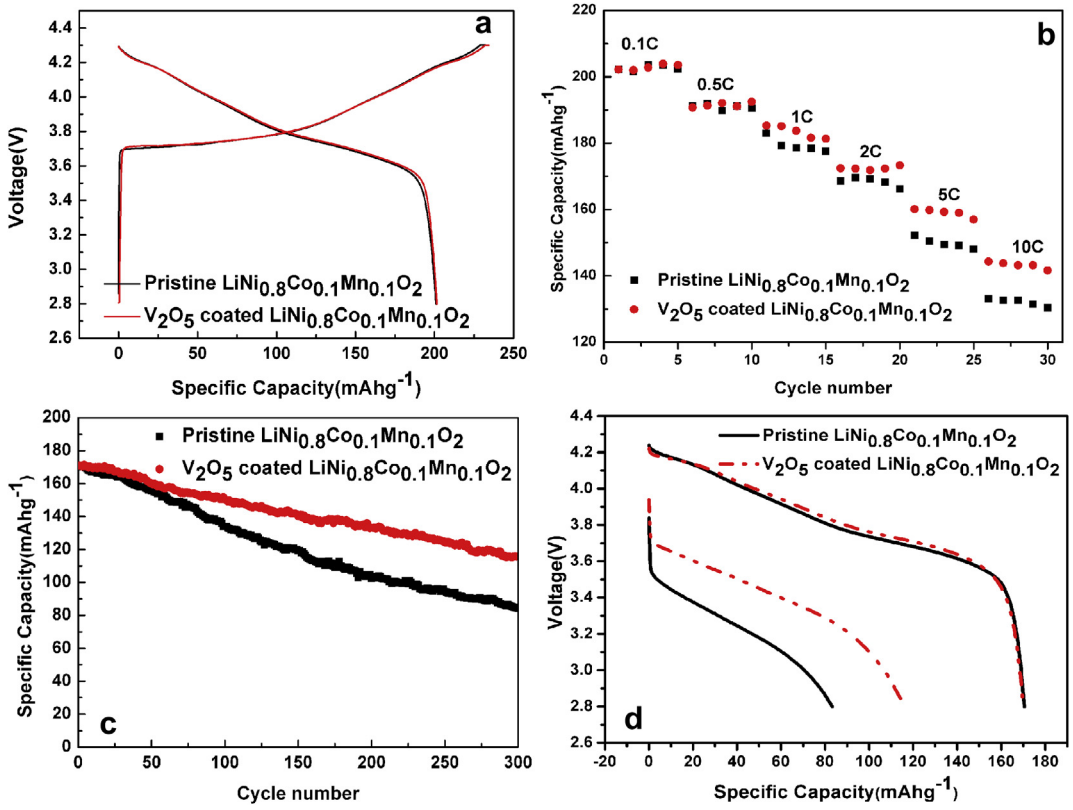

Fig. 5. (a) The initial charge/discharge curves of pristine and V_2O_5-coated sample at 0.1 C; (b) the discharge capacities of pristine and V_2O_5-coated sample at various currents (20–2000 mA g^{-1}); (c) the cycling performance of pristine and V_2O_5-coated sample cycled at 2 C; (d) the first and 300th discharge curves of pristine and V_2O_5-coated sample cycled at 2 C.

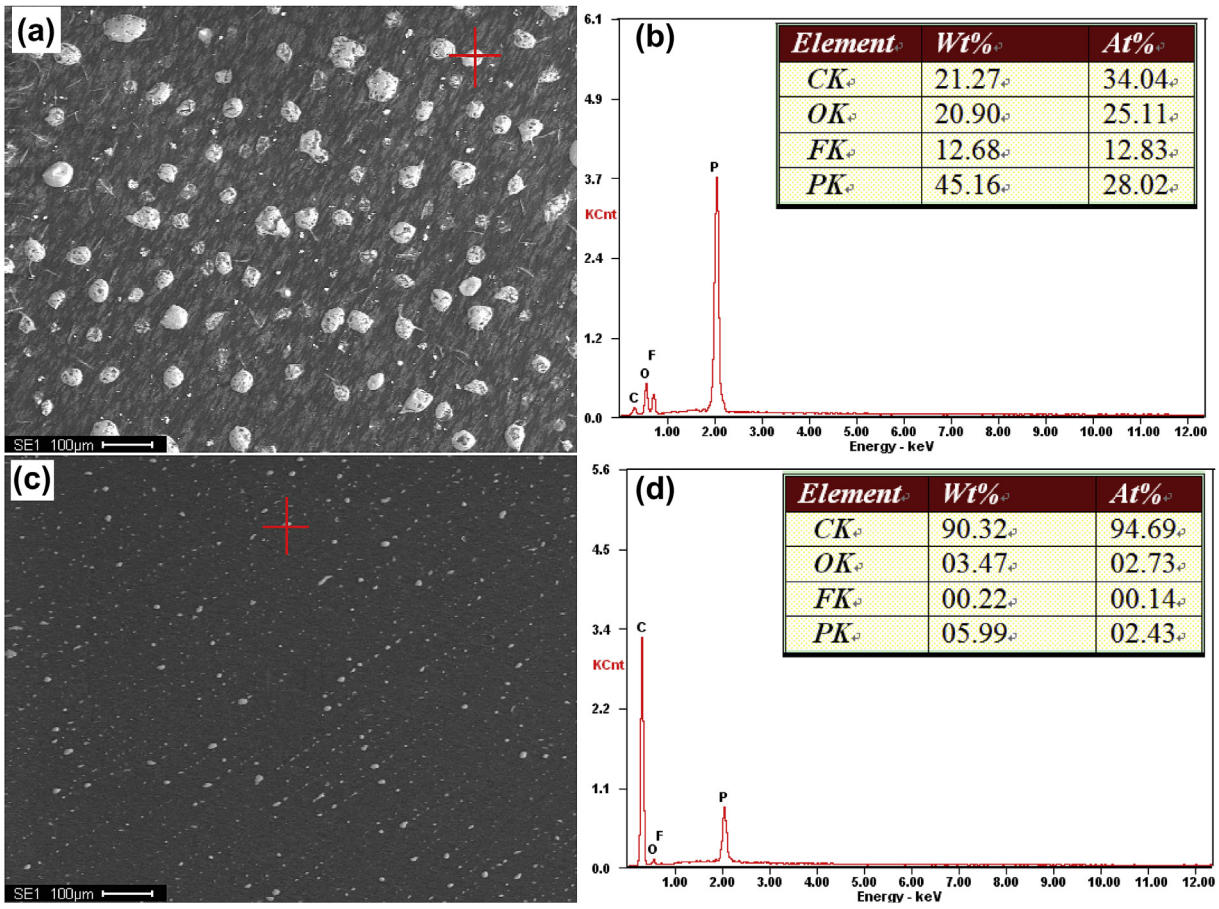

Fig. 6. Separator images of (a) pristine and (b) V_2O_5-coated $LiNi_{0.8}Co_{0.1}Mn_{0.1}O_2$ cells after extensive cycling at 60 °C; (b), (d) EDX analysis of chosen area in (a) and (c).

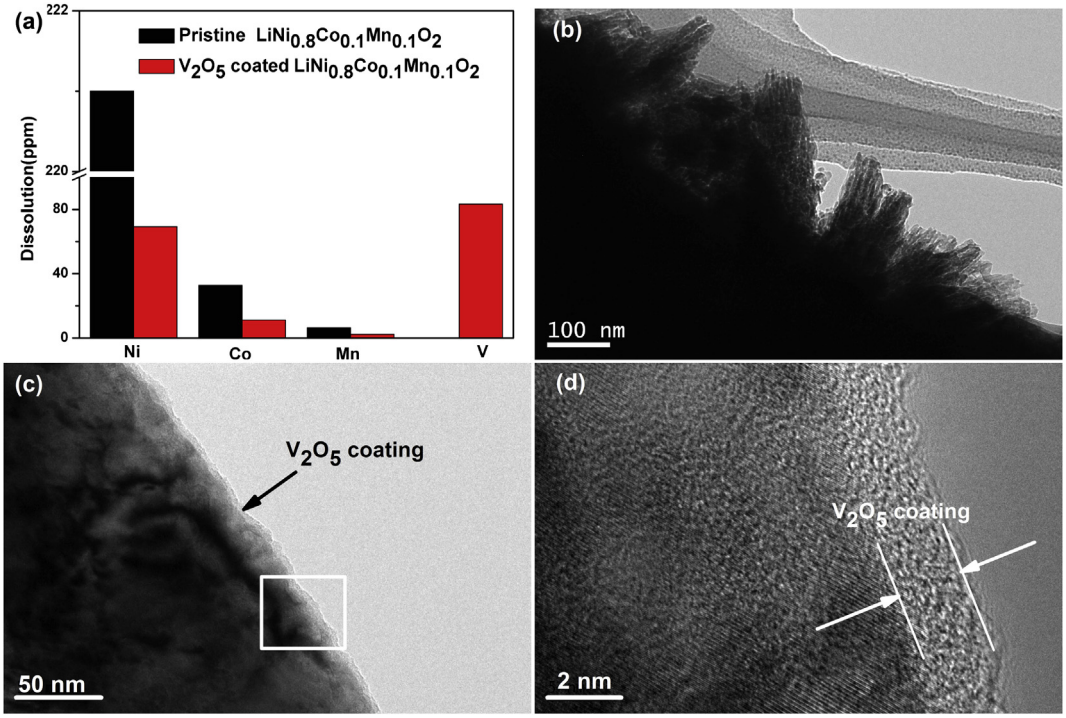

Fig. 7. (a) The concentration of metal dissolved in the electrolyte for pristine and V_2O_5-coated electrodes at 60 °C; TEM images of extensively cycled (b) pristine and (c) V_2O_5-coated electrodes; (d) HRTEM images of the selected area in (c).

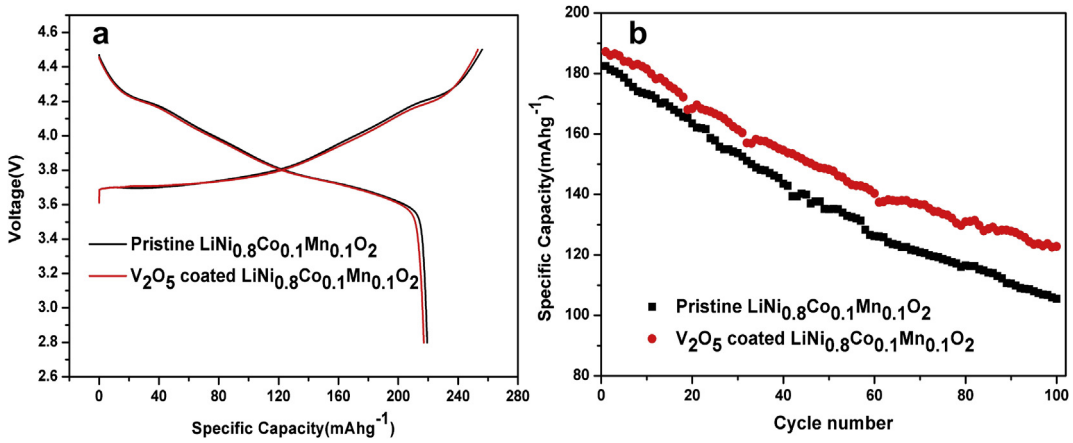

Fig. 8. The initial charge/discharge curves (a) and cycling performance (b) of pristine and V_2O_5-coated sample between 2.8 and 4.5 V.

inhibitor to enhance battery performance, which is not exist for other metal oxide coating (Al_2O_3, ZnO, ZrO_2), metal phosphate ($AlPO_4$, $Ni_3(PO_4)_2$) or fluoride coating (AlF_3, CaF_2). Because these coating materials hardly react with Li impurities after fired below 700 °C and Li impurities still adhere to the surface of $LiNiO_2$-based materials.

In fact, $LiPF_6$-based electrolyte contains a small amount of water and the water amount is greatly propagated from the decomposition of $LiPF_6$ salt at elevated temperature. The existence of a small amount of water causes breakdown of the electrolyte accompanying by HF generation. Then transition metal elements dissolution can occur in the charge state, which is responsible for capacity fade during cycling. The electrodes charged to 4.3 V are carefully disassembled in a glove box and then the recovered active materials are stored in the electrolyte at 90 °C for 1 week. Fig. 7(a) shows the amounts of Ni, Co and Mn that dissolved into the electrolyte from the pristine is much higher. In contrast, the V_2O_5-coated material shows considerable amount of V dissolution into the electrolyte, with amounts of 83.3 ppm. Thus, it is clear that there is a significant suppression of transition metal elements in the V_2O_5-coated $LiNi_{0.8}Co_{0.1}Mn_{0.1}O_2$ electrode during storage at 90 °C. This is verified by TEM images of pristine and V_2O_5-coated materials after storage in the electrolyte at 90 °C for 1 week. The TEM images (Fig. 7(c)) clearly show that the thickness of coating layer reduce from 6–10 nm to 1–2 nm, which explains that V_2O_5 continuously works as an HF scavenger and protects the active material during storage. However, the surface of the pristine material is severely damaged. This protective effect of the coating layer from the reactive electrolyte may lead to enhanced electrochemical properties of the coated material.

The cutoff voltage has an influence on the electrochemical properties of the cathode material. Fig. 8 presents the charge/discharge curves of the pristine and V_2O_5-coated sample at 20 mA g^{-1} (0.1 C rate) in the voltage range of 2.8–4.5 V and the

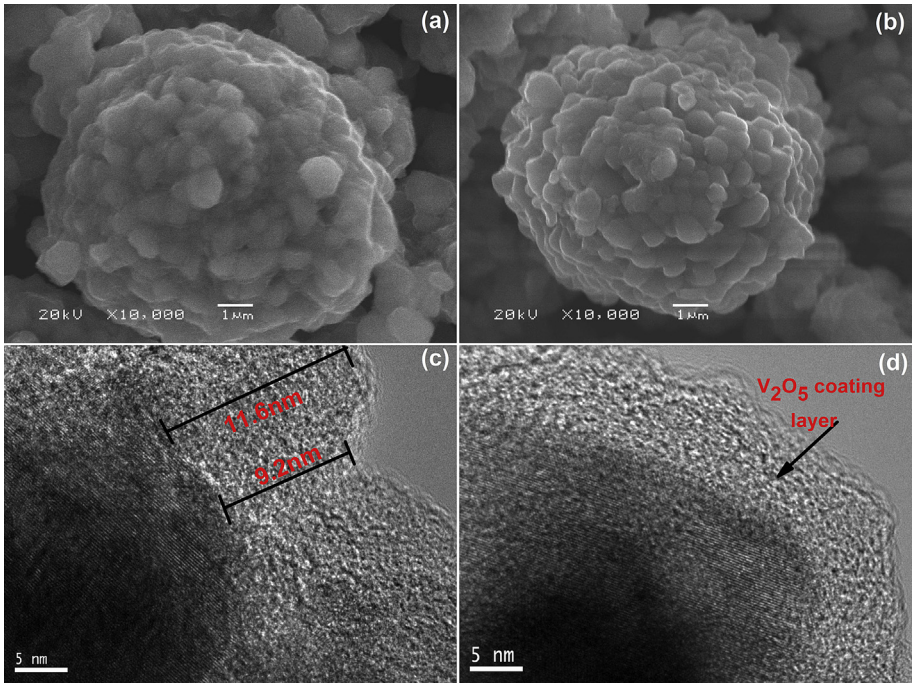

Fig. 9. SEM and HREM images of pristine (a, c) and V_2O_5-coated $LiNi_{0.8}Co_{0.1}Mn_{0.1}O_2$ (b, d) after storing in air for 30 days.

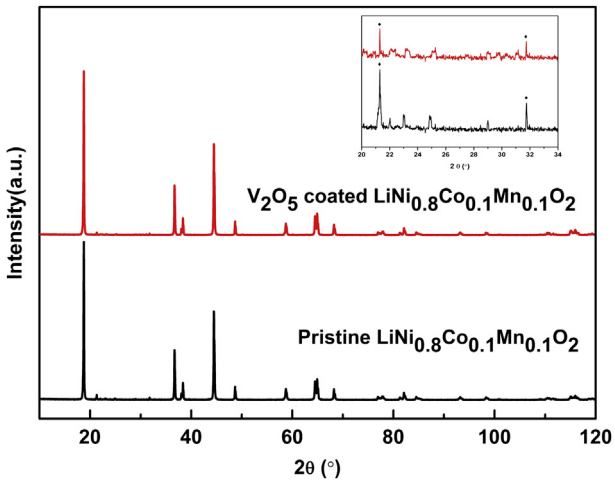

Fig. 10. XRD patterns of pristine and V_2O_5-coated sample after storage in air for 30 days.

corresponding capacity retention behaviours at 2 C. It is obvious that both cells show very stable and smooth charge/discharge curves, and the curves for both cells nearly coincide even up to the cutoff voltage of 4.5 V. This result indicates that the coating medium of V_2O_5 is not introduced into the bulk of $LiNi_{0.8}Co_{0.1}Mn_{0.1}O_2$ structure once again. Also, approximately 10% additional capacity is realized by extending the charge beyond the typical 4.3 V limit to 4.5 V. As expected, both cathodes decrease rapidly as the electrochemical cycling proceeded. The origin of this capacity fading is related to the increase in the surface reactivity between the highly oxidative Ni^{4+} and the electrolyte, resulting in significant interfacial impedance rise. The enhanced cycling performance is mainly ascribed to V_2O_5 coating layer which insulates the cathode from electrolyte.

From the above discussion, we can know a uniform and thin V_2O_5-coating layer is effective in improving the cycling performance and storage characteristics in electrolyte, which significantly works as HF inhibitor and/or HF scavenger. And we have succeeded to understand the enhanced battery performance at high voltage of V_2O_5-coated sample is related to the insulating role of V_2O_5 coating layer from electrolyte. However, a problem for scale-up with the $LiNiO_2$-based material is rapid moisture uptake upon exposure to air. Of course, it is worth studying the storage performance of V_2O_5-coated $LiNi_{0.8}Co_{0.1}Mn_{0.1}O_2$ in air.

A TEM micrograph of fresh $LiNi_{0.8}Co_{0.1}Mn_{0.1}O_2$ powder (Fig. 2(a)) shows good crystallinity at the edges of the grains. By contrast, particles from the air-exposed material (Fig. 9(c)) are covered by an apparently continuous layer at least 9.2 nm thick. Elemental analysis by EDX showed the coating to be composed primarily of carbon and oxygen, consistent with its identification as lithium carbonate by XRD (shown in Fig. 10). However, it is very difficult to observe a surface film on the coated sample because of the acidic coating layer.

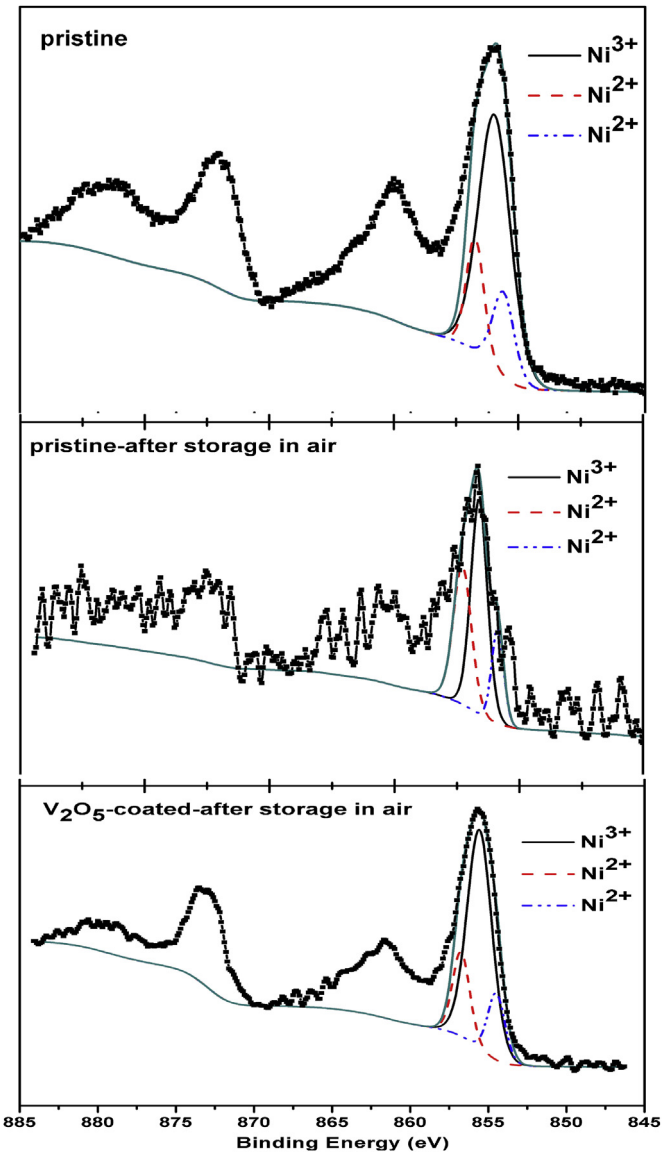

Fig. 11. XPS spectra of Ni2p taken from the surface of pristine and V_2O_5-coated sample after stored in air for 30 days.

Fig. 10 illustrates XRD patterns of pristine and V_2O_5-coated $LiNi_{0.8}Co_{0.1}Mn_{0.1}O_2$ after storage in air for 30 days. By Rietveld refinement (summarized in Table 1), both the lattice parameters *a* and *c* of the stored sample became larger than that of fresh sample and after storage in air, the degree of cationic disorder in pristine sample is more severe than V_2O_5-coated sample. It is worthwhile to note that the Ni at Li 3a site should be divalent due to the difference of ionic radius (r^{3+}_{Ni} = 0.56 Å, r^{2+}_{Ni} = 0.70 Å, and r^{+}_{Li} = 0.74 Å) [12].

Table 1
Rietveld analysis results of $LiNi_{0.8}Co_{0.1}Mn_{0.1}O_2$ before and after storage in air for 30 days.

Sample	*a* (Å)	*c* (Å)	Ni in Li site	$R_p/R_{wp}/R_{exp}$
Pristine sample	2.8710	14.1968	0.035	9.52/12.46/9.23
V_2O_5-coated sample	2.8709	14.1966	0.035	9.03/11.87/9.05
Pristine sample after storage	2.8958	14.2317	0.087	10.36/13.02/10.7
V_2O_5-coated sample after storage	2.8903	14.2112	0.052	10.04/12.49/9.52

Table 2
The relative area of Ni^{2+} and Ni^{3+} peaks in the pristine and coated electrodes before and after storage in air for 30 days.

Binding energy (eV) and Ni species	Pristine sample before storage (At.%)	Pristine sample after storage (At.%)	V_2O_5-coated sample after storage (At.%)
854.4 (Ni^{2+})	11.09%	10.72%	12.70%
855.5 (Ni^{3+})	70.03%	52.84%	65.28%
857.1 (Ni^{2+})	18.87%	36.44%	22.02%

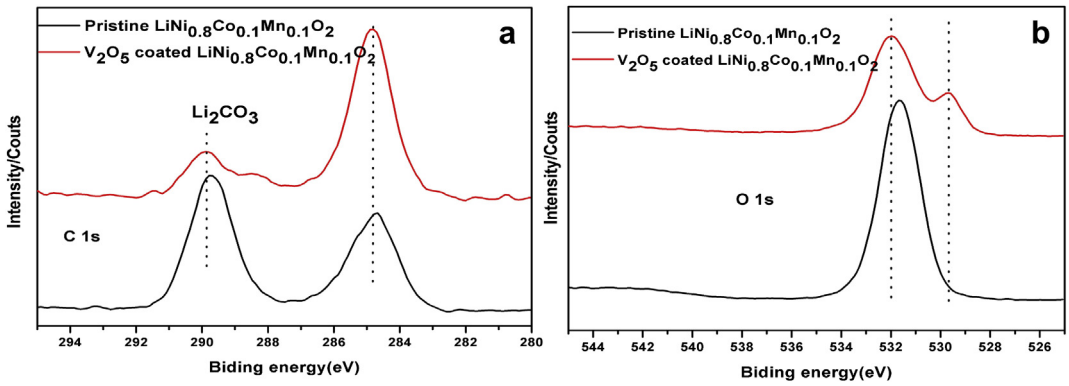

Fig. 12. XPS spectra of C1s (a) and O1s (b) taken from the surface of pristine and V_2O_5-coated sample after stored in air for 30 days.

Thus, XRD refinement results demonstrate that the change of ionic distribution and the Ni^{3+}/Ni^{2+} transformation on $LiNi_{0.8}Co_{0.1}Mn_{0.1}O_2$ during exposure to air also happens. However, Two weak peaks located at 21.2 and 31.6 which are identified as Li_2CO_3 phase appear in the XRD patterns of the stored samples, which is consisted with Yang's report and our previous report [12,30]. Additionally, the peak of Li_2CO_3 in pristine $LiNi_{0.8}Co_{0.1}Mn_{0.1}O_2$ is much more prominent. That's to say, V_2O_5-coating layer cannot prohibit the Ni^{3+}/Ni^{2+} transformation and lithium extraction altogether but play significant role in delaying them.

Further evidence for the increasing fraction of Li_2CO_3 and Ni^{3+}/Ni^{2+} transformation in the sample is observed by XPS of the pristine and V_2O_5-coated $LiNi_{0.8}Co_{0.1}Mn_{0.1}O_2$ after storage in air (shown in Fig. 11). The spectra of the cathodes between 858 and 852 eV can be deconvoluted into Ni^{2+} and Ni^{3+} peaks and are converted to their relative peak area. Table 2 summarizes the variation in the relative area percentage of Ni^{2+} and Ni^{3+}. Before storage, Ni^{3+} species are dominant, showing 70%. After storage in air for 30 days, relative areas of Ni^{2+} species increase, while the Ni^{3+} peak shows an opposite trend to Ni^{2+} for both samples. This result indicates that an increase in the fraction of Ni^{2+} species is accelerated with sacrificing Ni^{3+} species after storage. These Ni^{2+} species may have originated from the reduction of Ni^{3+} surface species. However, the fractions of Ni^{2+} in the V_2O_5-coated cathode are much lower than those of the pristine cathode after storage. In other words, the reduction process of Ni^{3+} to Ni^{2+} on the pristine $LiNi_{0.8}Co_{0.1}Mn_{0.1}O_2$ during storage is more severe, which will cause more active oxygen species and is the possible trigger for the chemical reactions to form Li_2CO_3/LiOH, as described in previous report on $LiNiO_2$.

The C1s and O1s XPS spectrums (displayed in Fig. 12) verify the surface structure changes on $LiNi_{0.8}Co_{0.1}Mn_{0.1}O_2$ during the storage. As mentioned above, the 289.3 eV peak in C1s spectra is attributed to a carbonate compound and the O1s peak at high binding energy can be assigned to nickel oxides and the impurity of adsorbed species [27]. Compared with coated sample, the C1s at 289.8 eV and O1s peak at high binding energy become more prominent, which implies more adsorbed species including Li_2CO_3. Furthermore, O1s peak at low binding energy of pristine sample disappears. This suggests that lattice oxygen is almost fully covered up by the adsorbed species or active oxygen species on the surface of the stored sample. So V_2O_5-coating layer the can slow down the Ni^{3+}/Ni^{2+} transformation and lithium extraction when storage in air.

What really aroused our interest to have a thorough study of the role of V_2O_5 coating layer is that it takes advantages over other oxide in improvement of storage performance in air. In our preliminary experiments, 0.5% V_2O_5-coated, 0.5% TiO_2-coated and 0.5% Al_2O_3-coated $LiNi_{0.8}Co_{0.1}Mn_{0.1}O_2$ were prepared by dissolving vanadiumoxy acetylacetonate, tetrabutyl titanate and aluminium isopropoxide in alcohol, respectively and followed by drying at 90 °C and annealing at 400 °C. The pH value of the powders (pristine, V_2O_5-, TiO_2- and Al_2O_3-coated samples) immersed in water is monitored by adding 20 g powder to 200 mL purified water with constant stirring with a magnetic stirrer. The pH value of pristine powders reaches as high as 12.85. Assuming the pH value is contributed by lithium impurities completely and no lithium leach from bulk, then a uniform coating of 1.5 wt.% LiOH adheres on all surfaces of the particles. This is contradictory with XPS and TEM results of pristine sample. So the high pH value of pristine in water is caused by lithium impurities and lithium leach from parent oxide. The TiO_2-coated and Al_2O_3-coated samples only show a little lower value, because lithium impurities are not removed even after TiO_2 and Al_2O_3 coating although lithium extraction is suppressed. However, the V_2O_5-coated sample shows the lowest value of pH at 11.24, indicative of a reaction of lithium impurities with the coating material during annealing.

Based on Table 3, it is speculated that V_2O_5 coating has superiority in weakening moisture uptaking ability in air when compared with TiO_2 and Al_2O_3 coating. After exposure to air for 30 days, the actual amount of LiOH/Li_2CO_3 on pristine $LiNi_{0.8}Co_{0.1}Mn_{0.1}O_2$ surface measured by titration method is 14367 and 1128 ppm and the amount of Ni in Li 3a site is found to increase from 0.035 for the fresh sample to 0.087 for the stored sample. The surface reaction mechanism may be described as follows [12]:

$$Ni^{3+} + O^{2-}_{(lattice)} \rightarrow Ni^{2+} + O^{-} \quad (4)$$

$$O^{-} + O^{-} \rightarrow O^{2-}_{(lattice)} + O \quad (5)$$

$$O^{-} + O \rightarrow O_2^{-} \text{ or } O + O \rightarrow O_2\uparrow \quad (6)$$

Table 3
The pH value and LiOH/Li_2CO_3 content in pristine and coated sample and after storage in air for 30 days (unit: ppm).

Sample	Before storage	After storage		
	pH	LiOH	Li_2CO_3	Ni in Li site
Pristine sample	12.85	1128	14367	0.087
V_2O_5-coated sample	11.24	590	3708	0.052
TiO_2-coated sample	12.31	754	6530	0.068
Al_2O_3-coated sample	12.25	772	6879	0.069

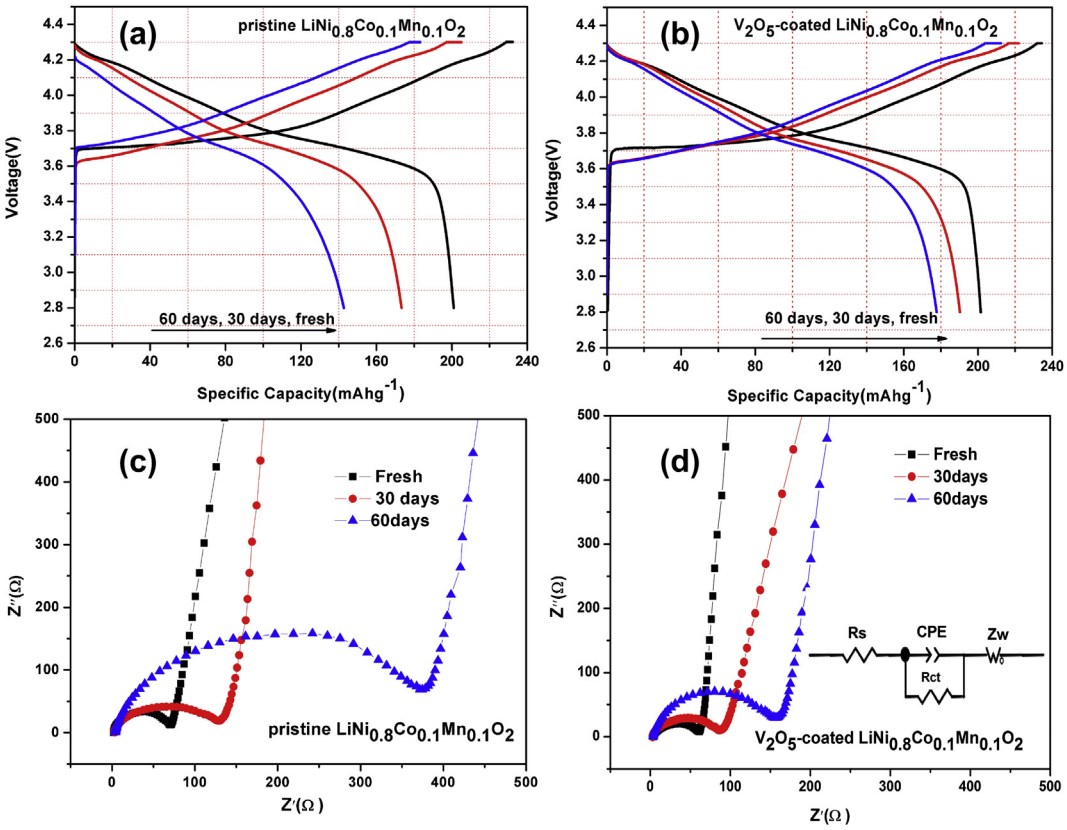

Fig. 13. The initial charge/discharge curves of pristine (a) and V_2O_5-coated samples (b); the Nyquist plots of pristine (c) and V_2O_5-coated samples (d) after storage in air for various time.

$$O^{2-}_{(\text{lattice})} + CO_2/H_2O \rightarrow {CO_3}^{2-}/2OH^- \quad (7)$$

$$2Li + {CO_3}^{2-}/2OH^- \rightarrow Li_2CO_3 + LiOH \quad (8)$$

All coated samples show much remarkably stable in air, especially for V_2O_5 coated sample. Ni^{3+}/Ni^{2+} transformation and lithium leach can be delayed by coating due to isolating the material from H_2O and CO_2. Nevertheless, lithium impurities still exist on the surface for TiO_2 or Al_2O_3 coated materials. Thus Li_2CO_3 forms and Li^+ ions can be more easily leached from the bulk when compared with V_2O_5 coated sample, because slightly acidic CO_3^{2-} ions are conducive to lithium leach.

Fig. 13 shows the first charge/discharge curves of pristine and V_2O_5-coated materials after storage in air for various times. Freshly synthesized samples both have a discharge specific capacity of 201 mAh g^{-1} in the voltage range of 2.8–4.3 V at a current density of 20 mA g^{-1}. However, the performance of pristine sample decreases dramatically after storage in air for 2 months, it drops from 201.2 to 143.3 mAh g^{-1}. The specific capacity of V_2O_5-coated electrode was initially much higher, 189.4 mAh g^{-1} after 1 month, and only decreased to 178.8 mAh g^{-1} after exposure in air for 2 months. In the mean time, both of the charge curves are 100–200 mV higher than that of the fresh sample, and the discharge curve is 100–200 mV lower than that of the fresh sample, indicating a larger electrochemical polarization for the stored material. This because the surface of $LiNi_{0.8}Co_{0.1}Mn_{0.1}O_2$ is covered by Li_2CO_3 after exposed in air and it may cause electronic disconnection due to the presence of an insulating coating or to physical separation and blocking of ions due to the presence of a surface layer with low ionic conductivity. Explicit evidence for a larger electrochemical polarization is found in the EIS (Fig. 13(c) and (d)) comparison of electrodes after exposure in air for different time. The resistances of both materials calculated through equivalent circuit increased with stored time and it is notable that the acceleration of the pristine electrode is more rapid.

4. Conclusions

Taking $LiNi_{0.8}Co_{0.1}Mn_{0.1}O_2$ as an example, we have tried to understand the improved battery performance and storage characteristics of V_2O_5-coated $LiNiO_2$-based cathode materials. The enhanced battery performance at cycling and high voltage is attributed to the lowered charge-transfer of the electrode. During the cycling and storage in electrolyte, V_2O_5 coating layer work as HF inhibitor and/or HF scavenger. Meanwhile, V_2O_5 works as isolating layer when cathode material contacts with electrolyte especially cycling at high voltage. Similar to other coating materials, the stability is significant enhanced by delaying Ni^{3+}/Ni^{2+} transformation and lithium leach from parent oxide when storage in air. However, V_2O_5 coating has superiority in suppressing moisture uptaking in air when compared with TiO_2 or Al_2O_3 coating, because only lithium-reactive V_2O_5 will consume the lithium impurities on $LiNiO_2$-based materials.

Acknowledgements

This study was supported by Major Special Plan of Science and Technology of Hunan Province, China (grant no. 2009FJ1002 & no. 2011FJ1005) and Hunan Provincial Innovation Foundation for Postgraduate.

References

[1] Y.K. Sun, S.T. Myung, B.C. Park, J. Prakash, I. Belharouak, K. Amine, Nat. Mater. 8 (2009) 320.
[2] M.-H. Kim, H.-S. Shin, D. Shin, Y.-K. Sun, J. Power Sources 159 (2006) 1328.
[3] R. Kostecki, F. McLarnon, Electrochem. Solid-State Lett. 7 (2004) A380.
[4] J. Shim, R. Kostecki, T. Richardson, X. Song, K.A. Striebel, J. Power Sources 112 (2002) 222.
[5] J.J. Saavedra-Arias, N.K. Karan, D.K. Pradhan, A. Kumar, S. Nieto, R. Thomas, R.S. Katiyar, J. Power Sources 183 (2008) 761.
[6] L. Croguennec, Y. Shao-Horn, A. Gloter, C. Colliex, M. Guilmard, F. Fauth, C. Delmas, Chem. Mater. 21 (2009) 105.
[7] J.J. Saavedra-Arias, C.V. Rao, J. Shojan, A. Manivannan, L. Torre, Y. Ishikawa, R.S. Katiyar, J. Power Sources 211 (2012) 12.
[8] G.V. Zhuang, G. Chen, J. Shim, X. Song, P.N. Ross, T.J. Richardson, J. Power Sources 134 (2004) 293.
[9] S.W. Song, G.V. Zhuang, P.N. Ross Jr., J. Electrochem. Soc. 151 (2004) A1162.
[10] K. Matsumoto, R. Kuzuo, K. Takeya, A. Yamanaka, J. Power Sources 81/82 (1999) 558.
[11] K. Shizuka, C. Kiyohara, K. Shima, Y. Takeda, J. Power Sources 166 (2007) 233.
[12] H.S. Liu, Z.R. Zhang, Z.L. Gong, Y. Yang, Electrochem. Solid-State Lett. 7 (7) (2004) A190.
[13] H.S. Liu, Y. Yang, J.J. Zhang, J. Power Sources 162 (2006) 644.
[14] G.-R. Hu, X.-R. Deng, Z.-D. Peng, K. Du, Electrochim. Acta 53 (2008) 2567.
[15] Y. Kim, J. Cho, J. Electrochem. Soc. 154 (6) (2007) A495.
[16] Y. Kim, H.S. Kim, S.W. Martin, Electrochim. Acta 52 (2006) 1316.
[17] S.-K. Hu, G.-H. Cheng, M.-Y. Cheng, B.-J. Hwang, J. Power Sources 188 (2009) 564.
[18] H. Cao, B. Xia, Y. Zhang, Xu, Solid State Ionics 176 (2005) 911.
[19] K.S. Park, A. Benayad, M.S. Park, W. Choi, D. Im, Chem. Commun. 46 (2010) 4190.
[20] J.W. Lee, S.M. Park, H.J. Kim, J. Power Sources 188 (2009) 583–587.
[21] M.G. Kim, H. Kim, J. Cho, J. Electrochem. Soc. 157 (7) (2010) A802.
[22] X.Z. Liu, P. He, H.Q. Li, M. Ishida, H.S. Zhou, J. Alloys Compd 552 (2013) 76.
[23] X.H. Xiong, Z.X. Wang, H.J. Guo, Q. Zhang, X.H. Li, J. Mater. Chem. A 1 (2013) 1284.
[24] A.M. Andersson, D.P. Abraham, R. Haasch, S. MacLaren, J. Liu, K. Amine, J. Electrochem. Soc. 149 (2002) A1358.
[25] N.V. Kosova, E.T. Devyatkina, V.V. Kaichev, J. Power Sources 174 (2007) 965.
[26] S.-C. Yin, Y.-H. Rho, I. Swainson, L.F. Nazar, Chem. Mater. 18 (2006) 1901.
[27] R. Gottschall, R. Schollhorn, Inorg. Chem. 37 (7) (1998) 1513.
[28] D. Aurbach, J. Electrochem. Soc. 136 (1989) 906.
[29] K. Edström, T. Gustafsson, J.O. Thomas, Electrochim. Acta 50 (2004) 397.
[30] X.H. Xiong, Z.X. Wang, P. Yue, H.J. Guo, F.X. Wu, J.X. Wang, X.H. Li, J. Power Sources 222 (2013) 318.